J. Cent. South Univ. (2015) 22: 2493−2502
DOI: 10.1007/s11771-015-2777-2

Springer

Preparation of MnO_2 and calcium silicate hydrate from electrolytic manganese residue and evaluation of adsorption properties

LI Chang-xin(李昌新), ZHONG Hong(钟宏), WANG Shuai(王帅),
XUE Jian-rong(薛建荣), WU Fang-fang(武芳芳), ZHANG Zhen-yu(张振宇)

College of Chemistry and Chemical Engineering, Central South University, Changsha 410083, China

© Central South University Press and Springer-Verlag Berlin Heidelberg 2015

Abstract: Electrolytic manganese residue (EMR), a high volume byproduct resulting from the electrolytic manganese industry, was used as a cheap and abundant chemical source for preparing MnO_2 and EMR-made calcium silicate hydrate (EMR-CSH). The MnO_2 is successfully synthesized from the metal cations extracted from EMR, which can effectively recycle the manganese in the EMR. By the combination of XRD, SEM and EDX analysis, the as-prepared MnO_2 is found to exhibit a single-phase with the purity of 90.3%. Furthermore, EMR-CSH is synthesized from EMR via hydrothermal method. Based on the detailed analyses using XRD, FT-IR, FE-SEM, EDX and BET surface area measurement, the product synthesized under the optimum conditions (pH 12.0 and 100 °C) is identified to be a calcium silicate hydrate with a specific surface area of 205 m^2/g incorporating the slag-derived metals (Al and Mg) in its structure. The as-synthesized material shows good adsorption properties for removal of Mn^{2+} and phosphate ions diluted in water, making it a promising candidate for efficient bulk wastewater treatment. This conversion process, which enables us to fabricate two different kinds of valuable materials from EMR at low cost and through convenient preparation steps, is surely beneficial from the viewpoint of the chemical and economical use of EMR.

Key words: electrolytic manganese residue; manganese dioxide; calcium silicate hydrate; adsorption

1 Introduction

Electrolytic manganese residue (EMR) is a potentially harmful industrial solid waste that comes from the electrolytic manganese industry and has rarely been recycled in large quantities [1]. Since 2000, China has become the world's largest producer, consumer, and exporter of electrolytic manganese metal (EMM). China's EMM production capacity reached 2.11 million tons and its actual production reached 1.31 million tons [2−3]. Because EMR contains some heavy metal elements and compounds, it is highly questionable if the EMR generated is managed improperly. The common practice in China is to collect the EMR in open sites near the plants. These collection sites are often not well managed to prevent releases to the soils and surrounding areas. Accordingly, the current situation surrounding the disposal of EMR has become a serious concern that threatens our life because it may cause severe problems in the environment such as a potential pollution of surrounding soil and receiving water bodies by the leaching of hazardous heavy metals and particulate matter emissions into surrounding areas [4−7]. In addition, these collection sites occupy massive land resources [8−9]. High volume EMR resulting from large scale industrial activities has long been considered to be a burden, due to the high costs for their associated post-treatment, storage and disposal.

Owing to its mineral composition, EMR has been mostly recycled as hydraulic cement, concrete aggregate, road base, brickmaking materials in civil engineering work, as well as for the production of chemical fertilizers in agricultural field [10−12]. Yet, problems associated with disposal, such as the potential environmental impacts and the severe environmental regulations, make the recycling of slag difficult. It is, therefore, essential to continuously develop new and advanced recycling processes of EMR.

According to the previous study, a novel conversion route for the production of two kinds of materials was developed in order to make full use of the chemical and economic potential of EMR. As especially rich in Mn and Ca content, EMR was used as a low-cost and abundant precursor for preparing MnO_2 and a calcium silicate hydrate (EMR-CSH), as illustrated in Fig. 1.

Foundation item: Project(21376273) supported by the National Natural Science Foundation of China; Project(2010FJ1011) supported by the Research Fund of Science and Technology of Hunan Province, China
Received date: 2014−06−13; **Accepted date:** 2014−09−15
Corresponding author: ZHONG Hong, Professor, PhD; Tel: +86−731−88830654; E-mail: zhongh@csu.edu.cn; WANG Shuai, Associate Professor, PhD; Tel: +86−731−88830654; E-mail: wangshuai@csu.edu.cn

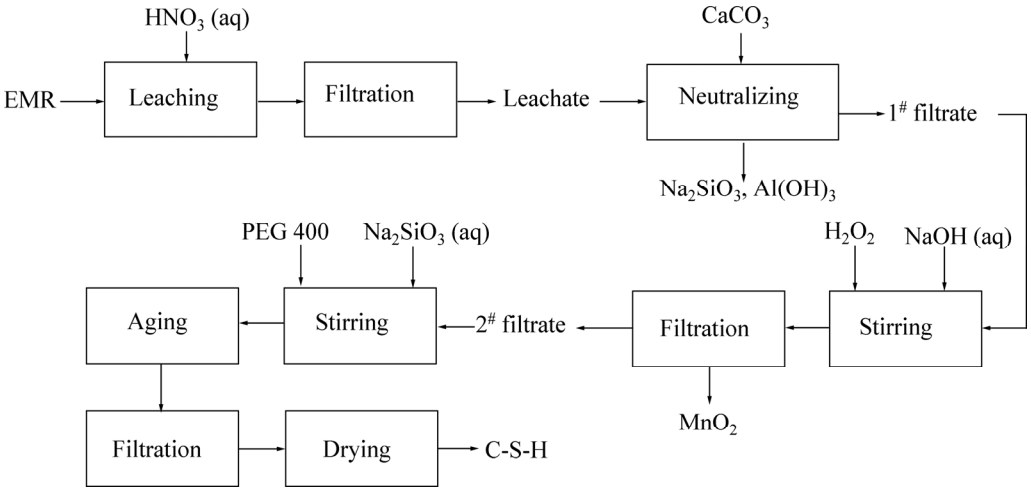

Fig. 1 Schematic diagram of synthetic routes from EMR to various mineral compounds

As there is rather high Mn content in EMR, about 4% (mass fraction) in general, sometimes even as high as 15% [7], the untreated discharge results in a huge loss of precious manganese element. In recent years, recovery of Mn from waste slags draws increasing attentions due to the growing scarcity of natural resources and environmental protection [13−14]. In this work, two-stage method was adopted to prepare MnO_2 [15−17]. The mineralogical composition and microstructure of the as-obtained MnO_2 were investigated in detail by XRD, SEM and EDX.

Calcium silicate hydrate (generally called C-S-H) is one of the components found in cement minerals and includes many amorphous and metastable structures [18−19]. On the basis of previous studies, C-S-H generally shows a high surface area and contains surface hydroxyl groups and hydrated Ca^{2+} ions to which various chemical entities can be attached or ion-exchanged, thereby being effective in adsorbing metal ions and phosphate ions ($H_xPO_4^{(3-x)-}$) from aqueous solutions and hence in purifying wastewater [20−22]. The present work offers detailed synthesis, characterization and application of EMR-CSH. EMR-CSH was synthesized from the resulting 2# filtrate (see Fig. 1) by a precipitation method at high pH and PEG-400 (polyethylene glycol) was added as dispersing agent in the reaction mixture. Structures were identified by using XRD, FT-IR, FE-SEM and BET surface area measurement in detail. The effects of pH and temperature on the material structures were also investigated to optimize synthesis conditions. Furthermore, the synthesized product was applied for removal of manganese ions and phosphate ions from water in order to evaluate the availability as an adsorbent.

2 Materials and methods

2.1 Materials

The EMR investigated in this work was mainly generated in leaching process of the manganese ore (with part of residue generated in electrolytic cell process) at an electrolytic manganese company, situated in western Hunan province, China. The chemical composition of EMR used in this work is listed in Table 1. The raw slag

Table 1 Chemical components of EMR, leaching residue, leaching solution, 1# filtrate and 2# filtrate

Component	EMR[a]	Leaching residue
$w(Na_2O)$/%	2.7	0.1
$w(SiO_2)$/%	24.6	66.4
$w(Al_2O_3)$/%	12.2	15.8
$w(MgO)$/%	1.7	0.7
$w(Fe_2O_3)$/%	7.9	1.1
$w(K_2O)$/%	2.4	3.7
$w(CaO)$/%	8.6	0.2
$w(MnO)$/%	4.6	0.3
$w(TiO_2)$/%	0.4	1.2

Component	Leaching solution[b]	1# filtrate[b]	2# filtrate[b]
$c(Na^+)/(mg\cdot L^{-1})$	121.7	118.4	112.9
$c(Al^{3+})/(mg\cdot L^{-1})$	3667.3	18.9	10.5
$c(Mg^{2+})/(mg\cdot L^{-1})$	209.5	186.8	12.6
$c(Fe^{n+})$[c]$/(mg\cdot L^{-1})$	3492.5	21.5	1.4
$c(K^+)/(mg\cdot L^{-1})$	496.2	465.8	458.3
$c(Ca^{2+})/(mg\cdot L^{-1})$	2920.8	4816.6	4699.2
$c(Mn^{2+})/(mg\cdot L^{-1})$	1889.9	1845.8	3.6

a: Determined by XRF analysis; b: Determined by ICP analysis; c: Fe includes multivalent species and content of Fe^{2+} accounts for 0.925% of total iron in leaching solution.

mainly consists of Al_2O_3, SiO_2, CaO, MnO and Fe_2O_3. This chemical composition is fairly common in EMR produced in China's EMM industry. Meanwhile, the phase composition of EMR is shown in Fig. 2 and the phase is very complex in the EMR as shown by X-ray diffraction (XRD). All experiments were performed using the same batch of EMR.

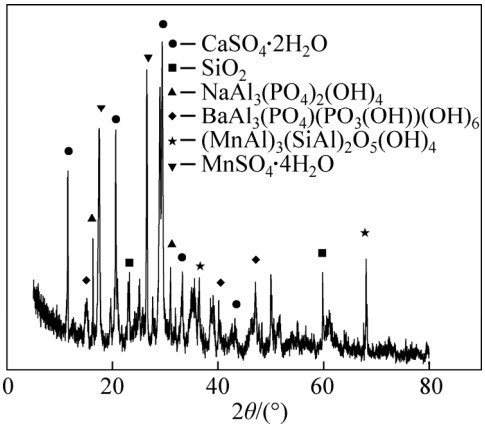

Fig. 2 XRD pattern of EMR

2.2 Synthesis of MnO_2

Prior to synthesis of MnO_2, the raw slag was ball-milled and screened using a 50 mesh sieve to facilitate dissolution. First, 10.0 g of the ball-milled slag was dissolved in 200 mL of 2 mol/L HNO_3 aqueous solution, and subsequently the temperature was elevated to 50 °C and stirred for 2 h to achieve a complete dissolution of EMR. The obtained suspension was separated into leaching residue and leachate containing plenty of metallic elements by filtration. The major chemical composition of the obtained leaching solution is shown in Table 1. Compared to liquid–liquid extraction, precipitation appears to be a simpler and cheaper method to separate metals. Therefore, to the as-obtained leaching solution, the pH was adjusted to (5.0±0.1) by $CaCO_3$ so that Fe and Al could be typically removed by hydroxide precipitation. After liquid and solid separation, the $1^{\#}$ filtrate was gained, as shown in Fig. 1 and the chemical composition is listed in Table 1.

The synthesis of MnO_2 was conducted based on a previous study [15−17]. The synthesis of MnO_2 was conducted on the $1^{\#}$ filtrate in 250 mL high-density polyethylene flasks ($1^{\#}$ filtrate volume 100 mL) located in a water bath at 25 °C under constant stirring (300 r/min) for 60 min. A solution of 2 mol/L NaOH was added very slowly to the $1^{\#}$ filtrate to raise the pH up to 10 and then 0.2% H_2O_2 (volume ratios of H_2O_2 to $1^{\#}$ filtrate) was supplied to the as-obtained slurry. After reaction, the slurry was filtered by 0.45 μm cellulose acetate filter papers. The solid precipitates remained on the filter papers after filtration were dried in the oven at 80 °C for 4 h. The dried solid residue was then collected for further analysis to determine the crystalline phases and morphology by XRD and SEM.

2.3 Synthesis of EMR-CSH

On the basis of Fig. 1, the $2^{\#}$ filtrate was collected by filtration and the chemical composition is shown in Table 1. EMR-CSH samples were prepared by precipitation by gradually adding $2^{\#}$ filtrate into sodium silicate solution under stirring, which was pre-dissolved with PEG400 in distilled water (PEG400 concentration was 0.6 mL/L). Initial Ca/Si ratio was kept at 1.0 in this work according to KUWAHARA et al [21]. To the blended solutions, 1 mol/L NaOH aqueous solution was added dropwise and the pH value was adjusted to (12.0±0.1), followed by stirring for 2 h at 100 °C and aging at the same temperature for another 10 h. The as-obtained precipitate was separated by filtration and washed with a copious amount of distilled water to remove sodium and nitrate ions and any residual polymer. The precipitates were then washed with ethanol and dried at 100 °C in a oven for 7 h. In order to optimize synthesis conditions, EMR-CSH samples were synthesized at different pH values (11.0, 12.0 and 13.0) and temperatures (60 and 100 °C).

2.4 Characterization

The crystalline phases were determined by XRD (D8 Discover, Bruker, Germany). XRF spectroscopy (Axios, PANalytical, Holland) was used to determine the major chemical composition of EMR and leaching residue. The concentrations of metals in solutions were determined by ICP-AES (Optima 5300DV, Perkin-Elmer, USA). The morphology and particle size of the crystals were observed by field emission scanning electron microscopy (FE-SEM) (Mira3, Tescan, Czech Republic), equipped with an energy dispersive X-ray analyzer (X-max20, Oxford, UK), by which the elemental analysis was performed. The Fourier transform infrared spectra (FT-IR) were recorded on a Thermo Scientific Nicolet 6700 FT-IR spectrophotometer. Spectral analysis was performed over the range of 4000−400 cm^{-1}. The specific surface area was determined by the nitrogen adsorption method. Nitrogen sorption experiments were carried out at 77 K using ASAP2020 (Micromeritics, USA). The sample was degassed under vacuum at 673 K for 12 h prior to data collection. The samples were then immersed in liquid nitrogen at 77 K before the sorption measurements were taken. The BET equation was applied to determine the specific surface area.

2.5 Adsorption test of EMR-CSH

In this work, removal tests of two different types of adsorbates (manganese ions and phosphate ions) dissolved in water were performed to evaluate the

adsorption properties of the synthesized EMR-CSH. The adsorption performance of the adsorbents was evaluated by mixing 100 mg of the synthesized EMR-CSH with test solutions (100 mL) containing predetermined amounts of adsorbates in sealed quartz vessels placed on an incubator for up to 15 h at 300 r/min. The initial solution concentrations were arbitrarily adjusted to 4 mmol/L for Mn^{2+} and phosphate adsorptions with $MnSO_4{\cdot}H_2O$ and $Na_2HPO_4{\cdot}12H_2O$, respectively. The adsorption test for phosphate was performed at 25 °C and pH 7.0. Meanwhile, the Mn^{2+} adsorption was conducted at 25 °C and at pH 4.0 in order to prevent the precipitation of Mn^{2+} as $Mn(OH)_2$. A portion of the solution was collected at predetermined time intervals by filtration, and the residual concentration was determined using Shimadzu UV-vis spectroscopy. The equilibrium adsorption capacity q_e (mg/g) is calculated using the following equation:

$$q_e = (C_0 - C_e)V/m \quad (1)$$

where C_0 and C_e (mg/L) are the concentrations of the test solution at the initial stage and under equilibrium conditions, respectively, V (L) is the volume of the test solution and m (g) is the mass of the adsorbent used.

3 Results and discussion

3.1 Characterization of prepared MnO_2

3.1.1 XRD analysis

As seen in Table 1, the concentration of Mn in the 2# filtrate is negligible compared with that in 1# filtrate, indicating that almost all of Mn leached from EMR can be recycled in the form of MnO_2. Meanwhile, it is known that MnO_2 exhibits polymorphism with α, β, γ and δ forms, which depends on the conditions of synthesis. The crystal structures are generally believed to be responsible for their properties [23]. Therefore, to further determine the composition of the solid products after reaction, the crystalline phases of the solid products are illustrated by XRD in Fig. 3. As seen in Fig. 3, the product obtained from EMR exhibits a characteristic XRD pattern of γ-MnO_2 [23−24] and no other phase is detected, indicating the high purity of the final products.

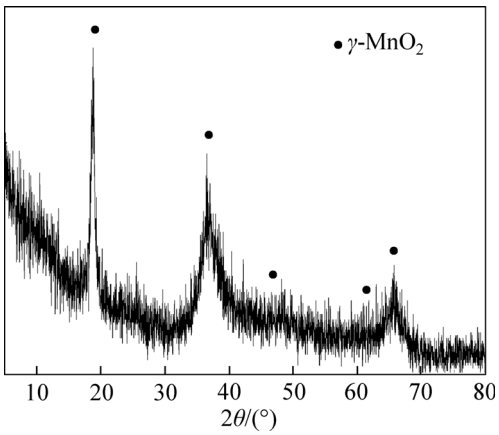

Fig. 3 XRD pattern of synthesized MnO_2

3.1.2 SEM and EDX analysis

SEM images and EDX spectrum of the as-prepared product, namely MnO_2, are depicted in Figs. 4 and 5. It is clearly shown that only irregular-shaped granular particles, which are mainly aggregates of small particles of submicrometer scale, are observed for the synthesized MnO_2 (Fig. 4(a)). Meanwhile, high magnification SEM image (Fig. 4(b)) presents a view of nanoparticles distributing uniformly along with some amorphous-like nanoparticles. It can be seen that the obtained products tend to assemble into nanoparticles with diameters of about 200 nm. The existence of these nanoparticles suggests a homogeneous nucleation process of γ-MnO_2 under the present experimental conditions. Moreover, the observation of γ-MnO_2 obtained in the present work (Figs. 4(a) and (b)) is similar to the study reported by WEI et al [24] and LI et al [23]. The EDX spectrum (Fig. 5) indicates the presence of Mn and O as the major elements. Meanwhile, peaks corresponding to Ca, Mg and Al are also present. And the origin of Ca, Mg and Al is EMR used as raw material in the synthesis process of MnO_2. As those elements are present at low concentration, they are not detectable in the XRD study (Fig. 3). Additionally, from the result of the EDX

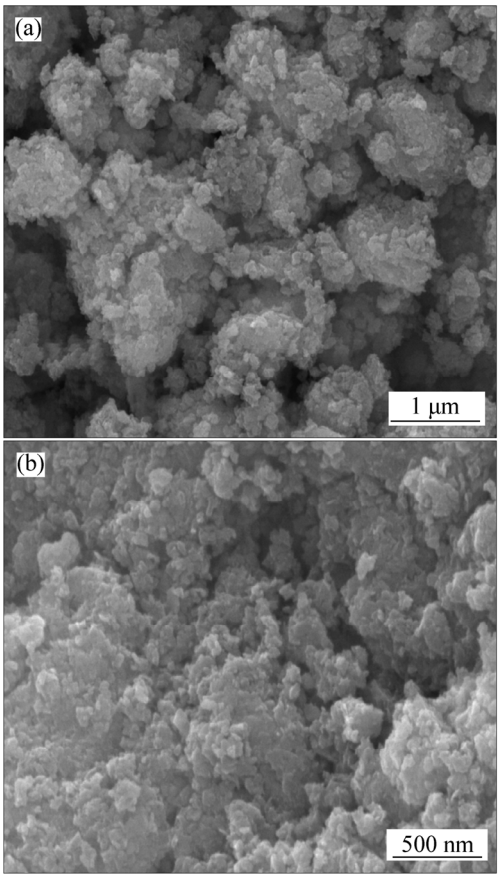

Fig. 4 FE-SEM images of synthesized MnO_2

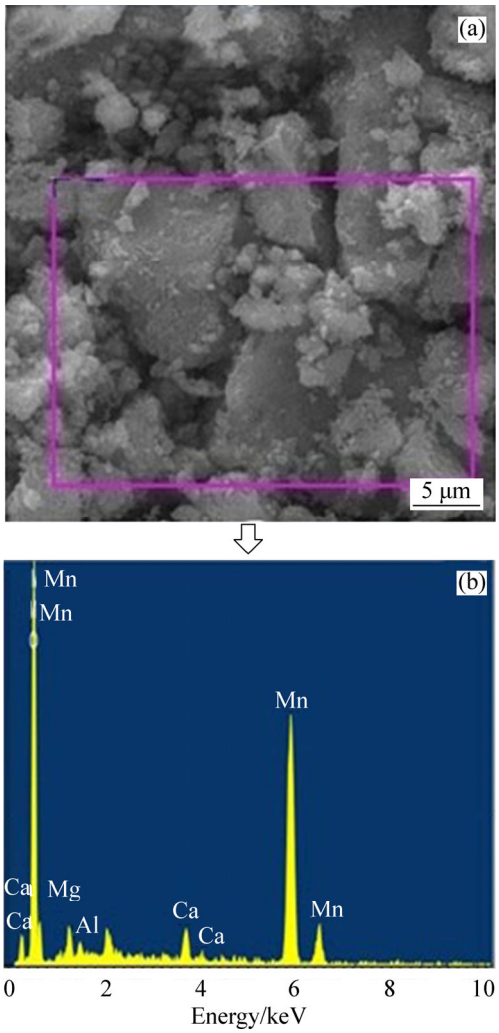

Fig. 5 EDX result of synthesized MnO_2

spectrum, the purity of MnO_2 obtained from 1# filtrate is about 90.3%.

Thus, these results ensure the availability of the synthesized MnO_2 as useful and reusable material [23−24]. The synthesized MnO_2 not only can be used as chemical product, namely commercial γ-MnO_2, in chemical industry directly, but also can be applied as raw material in manufacturing electrode materials.

3.2 Synthesis of EMR-CSH

3.2.1 Effect of synthesis pH

The concentrations of ions of each element in 2# filtrate extracted from EMR are listed in Table 1, showing that the 2# filtrate contains massive Ca^{2+} as well as other slag-derived metal ions. Hence, in order to optimize the use of resources, the EMR-CSH is prepared using 2# filtrate as Ca source of EMR-CSH. Figure 6 shows XRD patterns of EMR-CSH samples synthesized at different pH values at a fixed temperature of 100 °C. The hydration product synthesized at pH 11.0 shows the existence of calcite and portlandite, which is probably due to the fact that the portlandites have not tightly

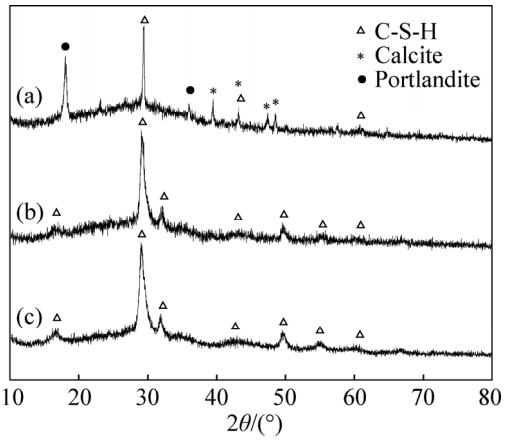

Fig. 6 XRD patterns of EMR-CSH synthesized at 100 °C at different pH values: (a) 11.0; (b) 12.0; (c) 13.0

bonded with SiO_4 tetrahedron under the condition of low basicity and calcite is generated from the reaction between those portlandites existing among the nanoparticles of C-S-H and CO_2 dissolving in the water [25−26]. With increasing the synthesis pH above 11.0, several distinct diffraction peaks appear. The samples synthesized at pH 12.0−13.0 particularly exhibit clear diffraction peaks at 2θ=16.6°, 29.2°, 31.9°, 49.5° and 54.9° which are well consistent with those reported in Ref. [27], suggesting a successful formation of C-S-H. This is due to the particle aggregation into the more thermodynamically stable arrangement induced by the high alkalinity. These results show that a precise control of the synthesis pH in this step drastically alters purity of the EMR-CSH, and that the most suitable pH for the synthesis of EMR-CSH is 12.0−13.0.

In addition to phase analysis from XRD patterns, a detailed analysis of the structure of EMR-CSH samples was performed by Fourier transform infrared spectroscopy (FT-IR). Figure 7 shows the IR spectra of EMR-CSH samples synthesized at different pH values. A series of EMR-CSH samples commonly exhibit distinct absorption bands. The silicate vibration regions of C-S-H spectra generally resemble those of 1.4 nm tobermorite, and all contain a characteristic set of bands centered at about 970 cm^{-1} [18]. This is the most intensive band in all the spectra, corresponding to the asymmetric and symmetric stretching vibrations of Si—O bonds in silicate tetrahedral units. With increasing synthesis pH, this band gradually shifts to lower wavenumbers (from 1025 to 973 cm^{-1}). Such a shift in infrared spectra can be explained by the formation of Si—O—Ca—O—Si linkages so as to compensate the positive charge of Ca^{2+} via a bonding to nonbridging oxygen (Si—O^-) [28−29]. The band at 1631 cm^{-1} is due to H—O—H bending vibration of molecular H_2O. The broad band at 3436 cm^{-1} is due to stretching vibrations of O—H groups in H_2O or hydroxyls with a wide range of hydrogen bond

strengths [28]. The presence of OH groups can be explained with a rapid and reverse absorption of atmospheric moisture and with the water content of the starting materials. The bands in the range of 1400−1500 cm^{-1} correspond to the asymmetric stretching of CO_3^{2-}, and the weak shoulder at around 876 cm^{-1} is due to the out-of-plane bending of CO_3^{2-} [18]. Meanwhile, the band appears at 454−469 cm^{-1}, which can be assigned to the deformation of TO_4 tetrahedra (T=Si, Al, Mg, etc) [21].

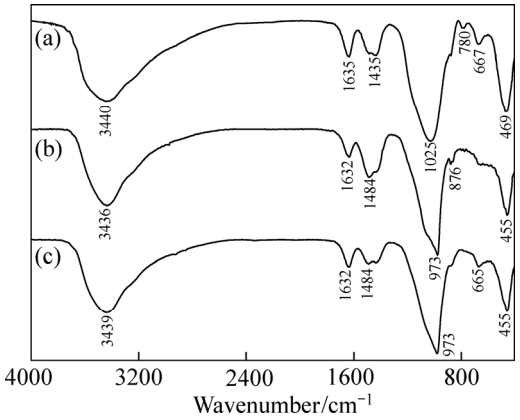

Fig. 7 FT-IR spectra of EMR-CSH synthesized at 100 °C and different pH values: (a) 11.0; (b) 12.0; (c) 13.0

3.2.2 Effect of synthesis temperature

The influence of synthesis temperature on the purity and structure was evaluated by means of XRD and FT-IR. Figure 8 shows the XRD patterns of EMR-CSH synthesized at two different temperatures at a fixed pH of 12.0. All samples exhibit diffraction peaks assignable to the C-S-H phase; however, EMR-CSH synthesized at 60 °C shows weaker peak intensities for C-S-H reflections and lower purity of C-S-H than the sample synthesized at 100 °C. This is due to the increased calcium hydroxide activity in solution triggered by the high temperature. In the IR spectrum (Fig. 9), the distinct peak shift of the band centered at 1024−973 cm^{-1}, which

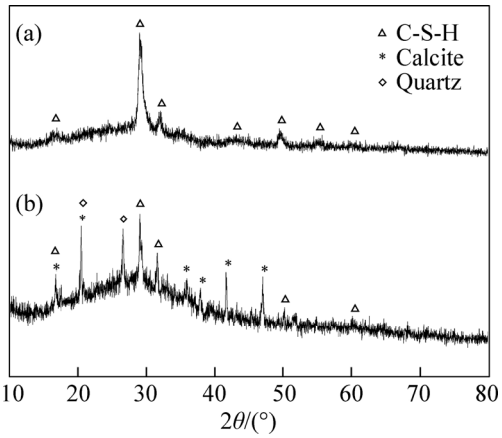

Fig. 8 XRD patterns of EMR-CSH synthesized at pH 12.0 and different temperatures: (a) 100 °C; (b) 60 °C

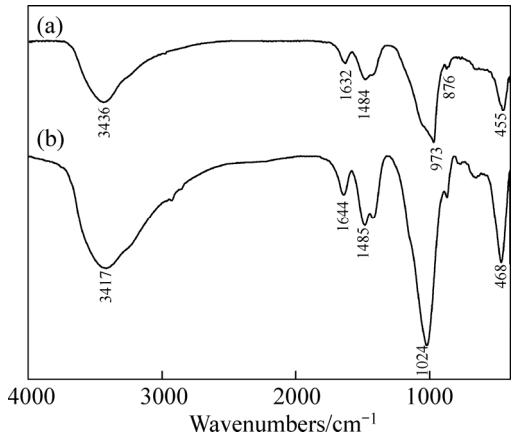

Fig. 9 FT-IR spectra of EMR-CSH synthesized at pH 12.0 and different temperatures: (a) 100 °C; (b) 60 °C

is associated with the new creation of Si—O—Ca bondings, is identified by increasing the synthesis temperature from 60 °C to 100 °C, elucidating the involvement of more Ca^{2+} ions into the C-S-H network structure at higher synthesis temperatures. Moreover, the lower synthesis temperature also induces an increased amount of CO_2 from air into reaction system, yielding additional bands attributable to CO_3^{2-} groups at around 1484 cm^{-1}. Therefore, for the synthesis of EMR-CSH by the $2^{\#}$ filtrate, the optimal temperature is 100 °C.

3.2.3 Results of BET surface area measurements

The results of the specific surface area and the pore volume of the EMR-CSH synthesized at pH 12.0 and 100 °C, being the best sample of this research, are shown in Table 2. The high surface area of synthesized EMR-CSH is a promising parameter for different applications such as adsorbent usages. Furthermore, C-S-H is well known to have a strong acid resistance capacity. From the viewpoint of employing this material as adsorbent, this specification might be useful for adsorbing metal ions in the highly acidic conditions without pretreatment.

Table 2 Structural parameters of EMR-CSH synthesized from $2^{\#}$ filtrate

Sample	$S_{BET}/(m^2 \cdot g^{-1})$	$V_{BET}/(cm^3 \cdot g^{-1})$
EMR-CSH	205	0.68

3.2.4 SEM analysis

The morphology and particle size of the EMR-CSH synthesized under optimal conditions (pH 12.0 and 100 °C) are observed by FE-SEM (Fig. 10). The FE-SEM image shows that EMR-CSH comprises nano-size plates, where the uneven plates with a diameter of approximately 200 nm are fused into an open framework structure with a “desert rose”-like surface morphology as shown in the SEM image. Meanwhile, microstructural analysis by SEM of the pore size in

Fig. 10 indicates that the pores are averaged between 100 and 500 nm in diameter around a larger open framework of about 1 μm in diameter. The open framework structure means that it has a large surface area and pore volume to which adsorbates are readily accessible. The observed morphological feature agrees well with that for pure C-S-H previously reported by JOHNSTON and SMALL [30], again elucidating the successful formation of C-S-H. The EDX image for the EMR-CSH grain synthesized at pH 12.0 and 100 °C is shown in Fig. 11. It is shown that SiO_2 and CaO are the major components in the EMR-CSH. And small fractions of Al and Mg are also detected by EDX spectrum. However, no detectable peaks attributable to Al and Mg compounds are observed in the XRD patterns. It is speculated that the compounds containing Al and Mg are either amorphous or too thin to possess the required long range order to show any crystalline form by X-ray diffraction.

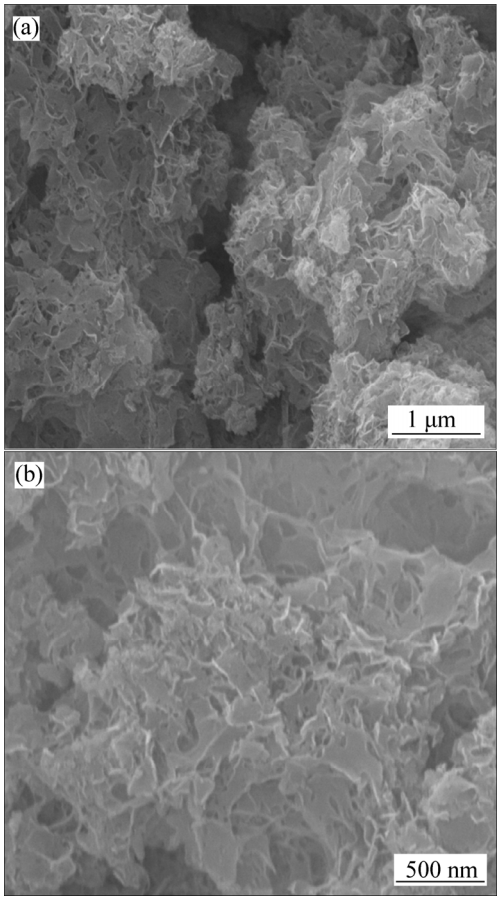

Fig. 10 FE-SEM images of EMR-CSH synthesized at pH 12.0 and 100 °C

3.2.5 Adsorption properties of EMR-CSH

For the conservation of environmental quality, many hazardous pollutants need to be removed from drinking water and water bodies such as rivers and lakes, where pollutants are present in the form of ions and chemicals from dyes, fertilizers, pesticides, oil and even sewage or

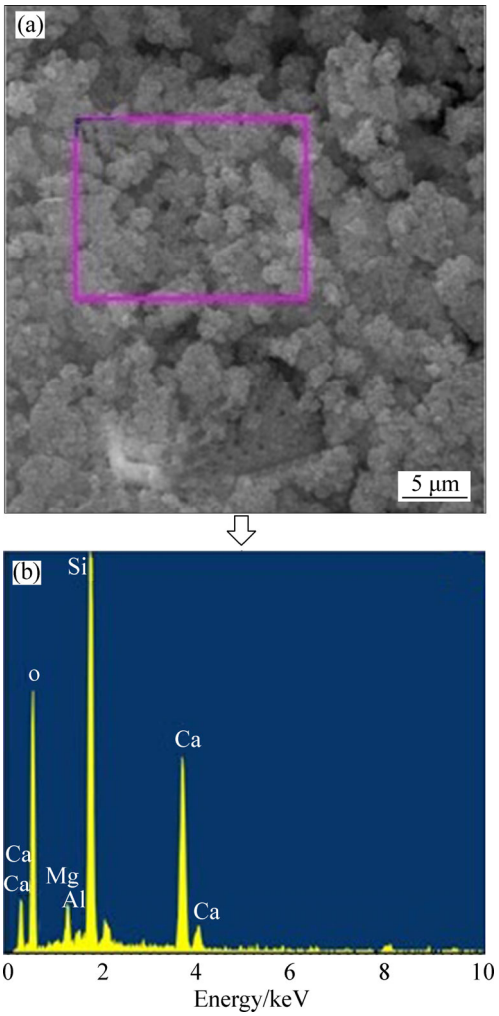

Fig. 11 EDX result of EMR-CSH synthesized at pH 12.0 and 100 °C

dirt. To date, many water purification methods have been developed such as chemical coagulation, flocculation, activated sludge formation, membrane separation and trickling filtration. Among them, physical adsorption using solid adsorbents has been a promising method for treating wastewater, owing to its advantages such as operational simplicity, low cost, availability in large amount and ability to treat pollutants in a sufficiently large-scale operation.

Since C-S-H contains abundant surface hydroxyls and hydrated Ca^{2+} ions, which act as efficient adsorption sites for various pollutants, it can potentially be used as a solid adsorbent in water purification. To assess the adsorption performance of the EMR-CSH, the removal of manganese ions and phosphate ions from water was tested. The adsorption uptake versus the adsorption time for two different types of adsorbates (Mn^{2+} and phosphate ion) diluted in water at 25 °C is shown in Fig. 12. In all adsorption systems, the concentrations of test solutions decrease with increasing time and then reach adsorption equilibrium almost within 15 h.

Figure 12(a) shows the adsorption uptake of Mn^{2+} as a function of adsorption time for EMR-CSH synthesized under optimal conditions (pH 12.0 and 100 °C). Over EMR-CSH compounds, Mn^{2+} adsorption immediately takes place within the first 200 min, and then reaches adsorption equilibrium, demonstrating that the EMR-CSH compound has a strong ability for binding metal cations. The fast Mn^{2+} removal rate at the initial stage is due to the fact that, initially, all adsorbent sites are vacant and the solute concentration gradient is high. The maximum adsorption uptake in 15 h for Mn^{2+} is 158.66 mg/g, indicating a quality high enough as an adsorbent. ICP analyses of the test solution recovered after the equilibrium adsorption reveal that 0.1 g of EMR-CSH has released 0.257 mmol of Ca^{2+} into the solution simultaneously with the adsorption of 0.288 mmol of Mn^{2+} during 15 h of adsorption. This result unambiguously indicates that the uptake of Mn^{2+} ions proceeds via an ion-exchange mechanism, i.e., the weakly bonded, network-modifying Ca^{2+} ions are released to the solution so as to replace Mn^{2+} ions.

A similar result is obtained in the adsorption of phosphate ions diluted in water (Fig. 12(b)). It is well-known that calcium-based materials have great potential for adsorbing phosphate ions from water owing to the strong affinity with phosphate ions to form insoluble calcium phosphate species [20−22]. Unlike the case of Mn^{2+} adsorption, EMR-CSH compounds still exhibit modest increases in the phosphate uptake even after 200 min, suggesting a slower adsorption rate than that for Mn^{2+} adsorption. This is conceivably due to the larger diffusion coefficient for phosphate adsorption than that for Mn^{2+} adsorption, which is derived from a larger ionic radius of phosphate ion. It is important to mention that when EMR-CSH compounds are used as adsorbents, the solution pH gradually increases from neutral to up to 10.0, where the dominant form of phosphate ion is HPO_4^{2-}. Meanwhile, the leaching amount of Ca^{2+} performed by ICP analysis in the test solution recovered after equilibrium adsorption is negligible. These results indicate that phosphate anions are adsorbed onto Ca^{2+} sites, probably via an electrostatic attraction between the positively charged Ca^{2+} sites and negatively charged HPO_4^{2-} anions, forming stable and dispersed calcium phosphate species on EMR-CSH surfaces.

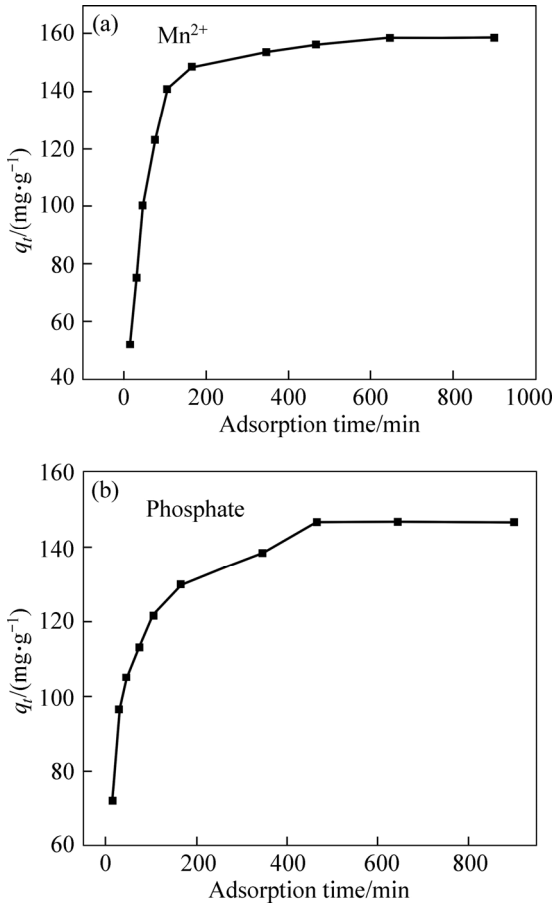

Fig. 12 Time course change in adsorption uptake of Mn^{2+} ions (C_0=4 mmol/L) (a) and phosphate ion (C_0=4 mmol/L) (b) diluted in water at 25 °C (Adsorbent dosage: 1.0 g/L)

To understand the adsorption process, the study of uptake kinetics is necessary as it provides valuable insights into both the reaction pathway and the rate-controlling mechanism of exchange reactions. In the present work, pseudo-first-order and pseudo-second-order kinetic models are employed to test the experimental data [21]. The pseudo-first-order and pseudo-second-order models are respectively described in the following equations:

$$\ln(q_e - q_t) = \ln q_e - k_1 t \quad (2)$$

$$\frac{t}{q_t} = \frac{1}{k_2 q_e^2} + \frac{t}{q_e} \quad (3)$$

where q_e and q_t are the amounts of adsorbate adsorbed on the adsorbents (mg/g) at equilibrium and at time t, respectively. k_1 (min^{-1}) and k_2 ($g \cdot mg^{-1} \cdot min^{-1}$) are the rate constants of pseudo-first-order and pseudo-second-order models, respectively.

The kinetic data are linearized using the pseudo-first-order and pseudo-second-order models, and plotted between $\ln(q_e - q_t)$ versus t and t/q_e versus t, respectively. The constants are calculated from the slope and the intercept of the plots, and are given in Table 3 and Table 4. The results in Tables 3 and 4 show that, for both Mn^{2+} and phosphate ions, the coefficients of determination (R^2=0.9995 and 0.9996) for pseudo-second-order model are much higher than those obtained using the pseudo-first-order model (R^2=0.8995 and 0.7240). As can be deduced from the disagreement between the calculated and experimental q_e values, the pseudo-first-order model can not fit the adsorption data well, suggesting that the adsorption onto EMR-CSH does not follow pseudo-first-order kinetics (see Table 3).

Table 3 Constants and correlation coefficients of pseudo-first order kinetic model for adsorption of different pollutants onto EMR-CSH

Adsorbate	q_e(exp)/(mg·g^{-1})	q_e/(mg·g^{-1})	k_1/min^{-1}	R^2
Phosphate	146.67	80.95	0.013	0.724
Mn^{2+}	158.66	110.68	0.012	0.8995

q_e(exp) and q_e are the experimental and calculated values of q_e, respectively.

Table 4 Constants and correlation coefficients of pseudo-second order kinetic model for adsorption of different pollutants onto EMR-CSH

Adsorbate	q_e(exp)/(mg·g^{-1})	q_e/(mg·g^{-1})	K_2/(g·mg^{-1}·min^{-1})	R^2
Phosphate	146.67	150.60	0.00031	0.9996
Mn^{2+}	158.66	164.20	0.00023	0.9995

q_e(exp) and q_e are the experimental and calculated values of q_e, respectively.

However, it can be seen from Table 4 that the calculated values of q_e using a pseudo-second-order model match well with the experimental q_e values, showing that the pseudo-second-order model fits the experimental data better than the pseudo-first-order model. Thus, the pseudo-second-order model explains the kinetic processes better.

This work shows that the synthesized EMR-CSH is highly-efficient as an adsorbent. Furthermore, the EMR-CSH adsorbent is easily recoverable from the water systems by a simple filtration, thereby demonstrating that the EMR-CSH can be used to remove hazardous pollutants from municipal and industrial wastewater.

4 Conclusions

A novel technology of preparation of MnO_2 and a calcium silicate hydrate (EMR-CSH) utilizing EMR as an abundant and cheap chemical source is developed. The MnO_2 is successfully synthesized from the metal cations extracted from EMR with the aim of recycling manganese according to cycle economical basis principle. The products, namely MnO_2, are investigated by XRD, FE-SEM and EDX. Results reveal that single-phase MnO_2 is formed and the purity of as-obtained MnO_2 is about 90.3%, which can be directly used as chemical product in chemical industry. Secondly, a calcium silicate hydrate is also synthesized from EMR by the hydrothermal method. Based on the detailed analyses using XRD, FT-IR, FE-SEM, EDX and BET surface area measurement, the product synthesized under the optimum conditions (pH 12.0 and 100 °C) is identified to be a calcium silicate hydrate with a specific surface area of 205 m^2/g incorporating the slag-derived metals (Al and Mg) in its structure. The as-synthesized material shows good adsorption properties for removal of Mn^{2+} and phosphate ions diluted in water, owing to the prominent adsorption or cation-exchange properties associated with the hydrated Ca^{2+} ions abundantly existing in its network structure.

It should be emphasized that this conversion process will offer novel solutions not only to waste management problems but also to environmental problems since the EMR poses a great risk to the environment by the leaching of hazardous heavy metals and particulate matter emissions into surrounding areas. Although more detailed works need to be done before practical applications can be realized, we believe that this process would be a key technology that offers novel solutions to waste management and environmental problems.

References

[1] HAGELSTEIN K. Globally sustainable manganese metal production and use [J]. Journal of Environmental Management, 2009, 90(12): 3736−3740.

[2] DUAN Ning, DAN Zhi-gang, WANG Fan, PAN Cen-xuan, ZHOU Chang-bo, JIANG Lin-hua. Electrolytic manganese metal industry experience based China's new model for cleaner production promotion [J]. Journal of Cleaner Production, 2011, 19(17): 2082−2087.

[3] LIU Tang-meng, ZHONG Hong, YIN Xin-rong. Research of resource utilization of electrolytic manganese slag [J]. China's Manganese Industry, 2012, 30: 1−6. (in Chinese)

[4] SUNDARAY S K, NAYAK B B, LIN S, BHATTAC D. Geochemical speciation and risk assessment of heavy metals in the river estuarine sediments—A case study: Mahanadi basin, India [J]. Journal of Hazardous Materials, 2011, 186(2): 1837−1846.

[5] YAN Chang-zhou, LI Qing-zhao, ZHANG Xian, LI Guo-xin. Mobility and ecological risk assessment of heavy metals in surface sediments of Xiamen Bay and its adjacent areas, China [J]. Environmental Earth Sciences, 2010, 60(7): 1469−1479.

[6] LIU Jing-ling, CHEN Qiu-ying, LI Yong-li. Ecological risk assessment of water environment for Luanhe River Basin based on relative risk model [J]. Ecotoxicology, 2010, 19(8): 1400−1415.

[7] LI Chang-xin, ZHONG Hong, WANG Shuai, XUE Jian-rong. Leaching behavior and risk assessment of heavy metals in a landfill of electrolytic manganese residue in western Hunan, China [J]. Human and Ecological Risk Assessment, 2014, 20(5): 1249−1263.

[8] HU Nan, ZHENG Ji-fang, DING De-xin, LIU Jun, YANG Lu-qing, YIN Jie, LI Guang-yue, WANG Yong-dong, LIU Yu-long. Metal pollution in Huayuan River in Hunan Province in China by manganese sulphate waste residue [J]. Bulletin of Environmental Contamination and Toxicology, 2009, 83(4): 583−590.

[9] DUAN Ning, WANG Fan, ZHOU Chang-bo, ZHU Chun-lei, YU Hong-bing. Analysis of pollution materials generated from electrolytic manganese industries in China [J]. Resources, Conservation and Recycling, 2010, 54(8): 506−511.

[10] ZHOU Zheng-guo, XU Long-jun, XIE Jin-lian, LIU Cheng-lun. Effect of manganese tailings on capsicum growth [J]. Chinese Journal of Geochemistry, 2009, 28(4): 427−431.

[11] WANG Jia, PENG Bing, CHAI Li-yuan, ZHANG Qiang, LIU Qin. Preparation of electrolytic manganese residue–ground granulated blast furnace slag cement [J]. Powder Technology, 2013, 241: 12−18.

[12] HOU Peng-kun, QIAN Jue-shi, WANG Zhi, DENG Cheng. Production of quasi-sulfoaluminate cementitious materials with electrolytic manganese residue [J]. Cement and Concrete Composites, 2012, 34(2): 248−254.

[13] LI Hui, ZHANG Zhao-hui, TANG Si-ping, LI Yan-an, ZHANG Yong-kang. Ultrasonically assisted acid extraction of manganese from slag [J]. Ultrasonics Sonochemistry, 2008, 15(4): 339−343.

[14] XIN Bao-ping, CHEN Bing, DUAN Ning, ZHOU Chang-bo. Extraction of manganese from electrolytic manganese residue by bioleaching [J]. Bioresource Technology, 2011, 102(2): 1683−1687.

[15] TAO Chang-yuan, SHA Ji-wen, LIU Zuo-hua, SUN Da-gui, DU Jun. Study on recovery of high valent maganese from $KMnO_4$ slag [J]. Chinese Journal of Environmental Engineering, 2011, 5(10): 2342−2346. (in Chinese)

[16] TAN Shi-yu, LUO Ting, ZHU Bi-jue. Study on the recycling of manganese dioxide in process of hydroquinone production by aniline oxidation [J]. Applied Chemical Industry, 2009, 38(10): 1542−1544. (in Chinese)

[17] PENG Tie-feng, XU Long-jun, CHEN Hong-chong. Preparation and characterization of high specific surface area Mn_3O_4 from electrolytic manganese residue [J]. Central European Journal of Chemistry, 2010, 8(5): 1059−1068.

[18] YU P, KIRKPATRICK R J, POE B, MCMILLAN P F, CONG X D. Structure of calcium silicate hydrate (C-S-H): Near-, mid-, and far-infrared spectroscopy [J]. Journal of the American Ceramic Society, 1999, 82(3): 742−748.

[19] RICHARDSON I G. The calcium silicate hydrates [J]. Cement and Concrete Research, 2008, 38(2): 137−158.

[20] ZIEGLER F, GIERE R, JOHNSON C A. Sorption mechanisms of zinc to calcium silicate hydrate: Sorption and microscopic investigations [J]. Environmental Science & Technology, 2001, 35(22): 4556−4561.

[21] KUWAHARA Y, TAMAGAWA S, FUJITANI T, YAMASHITA H. A novel conversion process for waste slag: synthesis of calcium silicate hydrate from blast furnace slag and its application as a versatile adsorbent for water purification [J]. Journal of Materials Chemistry A, 2013, 1: 7199−7210.

[22] SOUTHAM D C, LEWIS T W, MCFARLANE A J, JOHNSTON J H. Amorphous calcium silicate as a chemisorbent for phosphate [J]. Current Applied Physics, 2004, 4(2): 355−358.

[23] LI Gui-cun, JIANG Li, PANG Hong-tao, PENG Hong-rui. Synthesis of γ-MnO_2 single-crystalline nanobelts [J]. Materials Letters, 2007, 61(16): 3319−3322.

[24] WEI Ming-deng, KONISHI Y, ZHOU Hao-shen, SUGIHARA H, ARAKAWA H. Synthesis of single-crystal manganese dioxide nanowires by a soft chemical process [J]. Nanotechnology, 2005, 16(2): 245−249.

[25] SHEN Wei-guo, XIAO Li-qi, ZHAO Su-ling, ZHOU Ming-kai, MA Wei. Investigation on nano-scale microstructure of C-S-H with atomic force microscope [J]. Journal of the Chinese Ceramic Society, 2008, 36(4): 487−493.

[26] DONG Ya, LU Chun-hua, NI Ya-ru, XU Zhong-zi. Drug loading capacity and morphology controlling of hydration calcium silicate mesoporous spheres [J]. Bulletin of the Chinese Ceramic Society, 2012, 31(3): 511−515. (in Chinese)

[27] HE Yong-jia, ZHAO Xiao-gang, LU Lin-nu, STRUBLE L J, HU Shu-guang. Effect of C/S ratio on morphology and structure of hydrothermally synthesized calcium silicate hydrate [J]. Journal of Wuhan University of Technology: Mater Sci Ed, 2011, 26(4): 770−773.

[28] MEISZTERICS A, ROSTA L, PETERLIK H, ROHONCZY J, KUBUKI S, HENITS P, SINKO K. Structural characterization of gel-derived calcium silicate systems [J]. The Journal of Physical Chemistry A, 2010, 114(38): 10403−10411.

[29] YASUTAKA K, TAKATO Y, TAKASHI K, KOHSUKE M, HIROMI Y. Enhancement in adsorption and catalytic activity of enzymes immobilized on phosphorus-and calcium-modified MCM-41 [J]. The Journal of Physical Chemistry B, 2011, 115(34): 10335−10345.

[30] JOHNSTON J H, SMALL A C. Photoactivity of nano-structured calcium silicate–titanium dioxide composite materials [J]. Journal of Materials Chemistry, 2011, 21(4): 1240−1245.

(Edited by YANG Bing)